Radiation Measurements 92 (2016) 59–71

Contents lists available at ScienceDirect

Radiation Measurements

journal homepage: www.elsevier.com/locate/radmeas

Coded-aperture imaging systems: Past, present and future development – A review

Michał J. Cieślak [a, *], Kelum A.A. Gamage [a], Robert Glover [b]

[a] Department of Engineering, Lancaster University, Lancaster, LA1 4YW, UK
[b] Radiometric Systems Group, Sellafield Ltd, Seascale, CA20 1PG, UK

HIGHLIGHTS

- We present a review of the existing coded-aperture based radiation detectors.
- Highlight potential improvements to coded-aperture neutron imaging systems.
- Alternatives to 3He based neutron detection techniques are discussed.
- An investigation into pulse shape discrimination capable scintillators is performed.
- Requirements of neutron imagers for nuclear decommissioning are presented.

ARTICLE INFO

Article history:
Received 7 March 2016
Received in revised form
15 July 2016
Accepted 2 August 2016
Available online 3 August 2016

Keywords:
Coded-aperture
Neutron detection
Radiation imaging
Monte Carlo modelling

ABSTRACT

Scintillator based coded-aperture imaging has proven to be effective when applied for X- and gamma-ray detection. Adaptation of the same method for neutron imaging has resulted in a number of propitious systems, which could be potentially employed for neutron detection in security and nuclear decommissioning applications. Recently developed scintillator based coded-aperture imagers reveal that localisation of neutron sources using this technique may be feasible, since pulse shape discrimination algorithms implemented in the digital domain can reliably separate gamma-rays from fast neutron interactions occurring within an organic scintillator. Moreover, recent advancements in the development of solid organic scintillators make them a viable solution for nuclear decommissioning applications as they present less hazardous characteristics than currently dominating liquid scintillation detectors. In this paper existing applications of coded-apertures for radiation detection are critically reviewed, highlighting potential improvements for coded-aperture based neutron source localisation. Further, the suitability of coded-apertures for neutron imaging in nuclear decommissioning is also assessed using Monte-Carlo modelling.

1. Introduction

Accurate localisation of radioactive materials is crucial for nuclear safety and security. The growing threat of attacks using radioactive substances, as well as an increasing number of nuclear plants requiring characterisation to support decommissioning, necessitate development of a portable system capable of detecting radiation sources in real-time.

Radioactive substances are used in medicine, non-destructive testing, and power generation. For example, nuclear fuel used in power generation produces nuclear waste that needs to be carefully disposed of as it remains radioactive for a time period. If the source of radiation is not accurately identified and localised, radiation emitted by these materials can pose a health risk for personnel in close proximity to these materials. Localisation is particularly important during nuclear decommissioning and decontamination, since the actual location of the radioactive source within nuclear waste is often unknown.

Highly-penetrating radiation may be released in a form of X- or gamma-ray photons or free neutrons, emitted as a result of nuclear processes occurring within the atomic structure of radioisotopes. All three types of radiation mentioned can be detected using different gas filled tubes, which are sensitive to a specific type (Jahoda et al., 2006; Vanier, 2004); examples are ionisation

* Corresponding author.
E-mail address: m.cieslak@lancaster.ac.uk (M.J. Cieślak).

http://dx.doi.org/10.1016/j.radmeas.2016.08.002

chambers, proportional counters and Geiger-Mueller counters. Scintillators can also be used in the same way as primary detectors to detect each type of radiation (Tous et al., 2011; Woodring et al., 2003; Nakamura et al., 2009). They transform energy detected into light pulses that can be counted by photosensitive electronic components e.g. photodiodes and photomultiplier tubes (PMTs).

Although the detectors mentioned above generally provide good radiation sensitivity, by themselves, they offer no specific information about the location of the radioactive source. Preliminary results of a recent study by Schuster and Brubaker (Schuster and Brubaker, 2015) suggest that the anisotropic response of crystalline scintillation materials to neutron interactions may reveal some directional information about the source location. This type of information is of vital importance for nuclear decommissioning applications.

Substances used in the types of detectors mentioned can be difficult to source. ^{3}He, for instance, is mainly obtained as a byproduct from the radioactive decay of tritium; BF_3, on the other hand, is a hazardous gas and as such not desirable (Kouzes et al., 2010). Radiographic film represents a safe implementation of radiation detector. For example, it has been employed in medical devices to perform skeletal body scanning with X-rays, successfully identifying fracture location (Lilley, 2001). A modification to the film detector, in the form of an imaging plate, allows detection of radioactive sources, where it is particularly useful for nuclear decommissioning applications (Hirota et al., 2011; Masumoto et al., 2002).

Radiation imaging methods do not only detect an occurrence of a radioactive event but also provide the location of the incident. As such their potential has led to the development of radiation cameras – based on the operation principle of a general pinhole camera (Mortimer et al., 1954). Pinhole cameras, capable of identifying radioactive substances from a distance, are frequently used in nuclear decommissioning. CARTOGAM is an example of such gamma-ray pinhole imager (Gal et al., 2000, 2001; Cattle et al., 2004). The size of the pinhole determines the angular resolution and signal-to-noise ratio (SNR) of a specific camera; the former increases in a camera with a small opening, whereas the latter decreases when the diameter of a pinhole is decreased.

It follows that an ideal single pinhole camera, would require an infinitely small pinhole to obtain the highest angular resolution. Conversely, the highest SNR would be achieved in a camera with an infinitely long diameter of the opening. Hence, in practical applications, a compromise must always be found between SNR and the angular resolution for the single pinhole cameras. In order to address this problem scatter-hole cameras were developed, where multiple holes of small diameter were distributed randomly on the aperture offering significant improvements in SNR, while maintaining good angular resolution (Dicke, 1968). However, reconstruction of the original image was difficult due to the random distribution of the pinholes. The issue was addressed by coded-aperture imaging, which was introduced with 'encoding' and 'decoding' arrays to simplify the process of image reconstruction (Fenimore and Cannon, 1978).

Coded-aperture imaging is a technique adopted in X-ray cameras and telescopes, widely utilised in numerous space exploration missions (Gehrels et al., 2004; Hong et al., 2004; Tumerl et al., 1997; Del Monte et al., 2007; Feroci et al., 2007). Due to similar characteristics to X-rays, coded-aperture method has been incorporated into gamma-ray imagers for medical applications (Alnafea et al., 2006, 2007), non-destructive testing (Damato et al., 2007), explosives detection (Faust et al., 2009), as well as for nuclear decommissioning and decontamination; these are GAMPIX (Gmar et al., 2011), RADCAM (Woodring et al., 2003) and High-Energy Radiation Visualiser (HREV) (Sudarkin et al., 1996, 1998). Coded-aperture methods, for neutron source localisation, have been applied in the field of national security (Marleau et al., 2009; Woolf et al., 2012) and nuclear material detection at fuel cycle facilities (Hausladen et al., 46191).

The scintillator based coded-aperture neutron imaging systems mentioned target fast neutron localisation. In each case pulse shape discrimination (PSD) methods are exploited to separate gamma-rays from neutron events. Multiple channel real-time PSD has been successfully implemented laying the foundations for high resolution (high number of pixels) organic scintillator based coded-aperture imagers (Joyce et al., 2014). However, identified neutron interactions must be localised within the scintillator so that the decoding process can be performed. The decoding process, which may contribute to the timing overhead of the localisation procedure, is required to infer the actual location of the radioactive substances.

In this paper existing coded-aperture imaging systems are critically reviewed with relevance to radiation detection and localisation. The advantages of the coded-aperture technique over other methods are recognised, when used for X- and gamma-ray detection, as well as its potential for neutron imaging. Additionally, the coded-mask itself, as well as sensitive neutron detectors for such an application are also highlighted. The potential of employing coded-aperture based techniques for neutron imaging in nuclear decommissioning is evidenced by a simple model generated in Monte Carlo N-Particle eXtended (MCNPX) simulation software package.

2. Radiation imaging and development of collimator-based detectors

Radiographic film was the original method of X-ray detection, used by Roentgen to discover X-rays, that was later adopted for gamma-radiography. Radiographic film has been successfully implemented in medical devices to perform skeletal body imaging with X-rays. It was possible due to the attenuation properties of X-rays for elements such as Ca (Lilley, 2001). A modification in a form of an imaging plate was introduced to the film detector to map ^{239}Pu in human lungs (Hirota et al., 2011).

In medical applications, an X-ray radiation source is placed in front of an object to be imaged, whose shadow is cast on the photographic film, where the picture of the object is projected. Images generated using this method show good spatial resolution but low sensitivity. Replacing the film with a pixelated charge coupled device (CCD) offers a way of improving the low sensitivity issue. It allows an analogue to digital converter (ADC) to be connected to individual pixels on the device. The ADC can be adjusted to ignore signals below certain voltage threshold to reduce the amount of noise reconstructed, effectively increasing the sensitivity of such a device (Ott et al., 2000).

Semiconductor solid state detectors, for instance cadmium zinc telluride (CdZnTe), may also be implemented (either independently or in conjunction with gas filled tubes, scintillators) for radiation localisation. When solid state detectors are exposed to radiation sources directly, they convert the pulses - emitted as a result of the interaction between the radiating particles and the detector – into electrical current, which can be easily measured. Although semiconductor solid state detectors are more susceptible to damages caused by radiation, they are sometimes preferred in spectrometry applications due to their superior energy resolution (Knoll, 2010).

As an alternative to direct detection methods, ionising properties of specific gases prompted the development of detector tubes. The tubes filled with gas produce an electronic signal as a result of ionisation between the gas and radioactive particles (Knoll, 2010). Depending on the radiation type gases utilised include BF_3 and Xe

for neutron and X-, gamma-ray detectors respectively. Alternatively, the scintillating properties of specific chemical compounds, for example CsI(Tl) and CsI(Na), offer a way of transforming X- and gamma-ray energy to light photons that can be counted using photosensitive electronic components.

Scintillator, such as CsI(Tl), can be used as a sensitive detector for a single pinhole radiation camera (Baek et al., 2013). Spatial resolution of the pinhole camera depends predominantly on the size of the single opening in the aperture and the performance of the sensitive detector used. However, it can be significantly improved if a collimator is used to narrow the path of the incoming radiation to the single opening of the aperture (Islamian et al., 2015). Replacing the single pinhole camera with a multi hole version, which was then followed by a new family of coded-aperture imaging systems, enhanced the quality of images obtained even further.

2.1. Coded-aperture based imaging

The coded-aperture approach for radiation detection has its roots in development of scatter-hole cameras for X- and gamma-rays. Introduction of a multi-hole mask improves the SNR while maintaining a good angular resolution of a small diameter, single hole imaging device (Dicke, 1968). In mathematical terms masks were represented as binary arrays with the ones corresponding to the pinholes, and the zeros to opaque elements in the aperture. In the early work on coded-apertures, pinholes were randomly distributed on the mask and placed in front of a source to be analysed. The source casts multiple overlapping shadows on the detector through the mask as presented in Fig. 1. Fourier convolution theorem is then used to reconstruct a single, high resolution image from the photons counted on the detector plane (Ables, 1968). Since the pinholes were randomly distributed, a construction of a unique binary array was required for each specific application.

Random patterns pose difficulties with image reconstruction due to a lack of uniformity in pinholes distribution. An inherent noise appears as a result of small terms present in Fourier transform of large size random binary arrays. This problem was addressed by the development of uniformly redundant arrays (URAs). If the distribution of the transparent and opaque elements of the aperture can be represented as a binary encoding array A and the decoding array as G, then A and G can be chosen such that the reconstructed image (correlation of A and G with addition of some noise signal N) approximates a delta function. Delta function is represented by a single impulse located at the central point in signal analysis. In radiation detectors the impulse indicates the location of the reconstructed source (Poularikas, 2006).

Calculation of possible dimensions of the arrays is based on pseudo-noise arrays and previous research documents their implementation for URA based coded-apertures. It has experimentally been shown that URAs offer significant improvements to SNR in comparison with randomly distributed arrays; the quality of reconstruction is improved if the exposure time is increased. URA based coded-apertures are constructed by 2×2 arrangement of the basic design (Fenimore and Cannon, 1978; Calabro and Wolf, 1967). Thus, the size of the detector can be kept small as only the basic array is required to fully recover the source distribution.

Despite its advantages the algorithm used for the construction of URAs restricts the shape of the aperture to a rectangle as vertical and horizontal sides dimensions, p and q, must satisfy the condition $p - q = 2$ (Fenimore and Cannon, 1978). This limitation was recognised and a modification to the original design was introduced in a form of a hexagonal URA (HURA). An algorithm, based on pseudo-noise (PN) sequences (MacWilliams and Sloane, 1976), for the realisation of URA on a hexagonal lattice was first presented by Finger and Prince (Finger and Prince, 1985). It followed a previously proposed implementation of a rotating HURA for gamma-ray imaging (Cook et al., 1984). In the new form HURA was successfully adopted for X- and gamma-ray imaging in high energy astronomy (Goldwurm et al., 1990). In addition a set of characteristics to assess the performance of the aperture was also proposed (Caroli et al., 1987).

The limitation imposed on the physical dimensions of the coded-aperture designs based on URA algorithm led to the development of another class of coded-aperture arrays. Pseudo-Noise Product (PNP) arrays allowed a construction of coded-apertures in previously unavailable dimensions. PNP array can be implemented in any dimensions, provided a corresponding PN sequence exists. However the transparency of PNP arrays is halved in comparison to URAs, because a two-dimensional PNP array is constructed through a direct product of two one-dimensional PN sequences. Although the resulting transparency of the coded-aperture is reduced to 25%, SNR comparison with other techniques shows that PNP arrays achieve superior results to pinhole cameras and only slightly inferior to URAs (Gottesman and Schneid, 1986).

Modified Uniformly Redundant Array (MURA), introduced with a change to URA's encoding algorithm, enabled new arrays to be created in linear, hexagonal and square configurations. The design method for URAs was modified, so that the new arrays were based on quadratic residues rather than PN sequences (Gottesman and Fenimore, 1989). Consequently, hexagonal MURA patterns differ significantly from the previously developed HURAs. The hexagonal

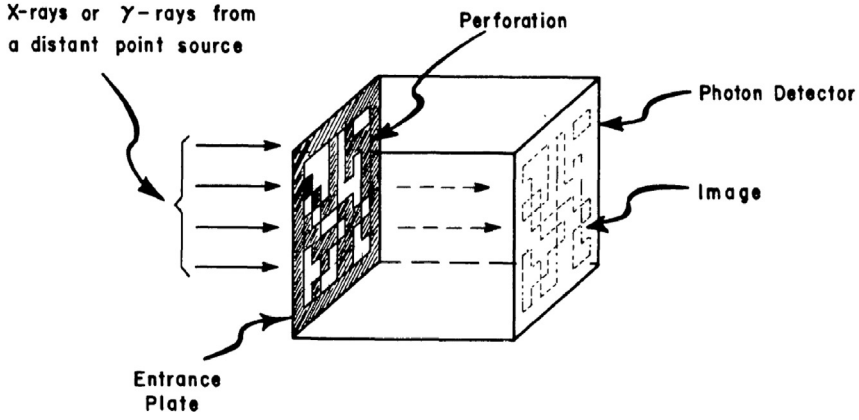

Fig. 1. Scatter-hole camera aperture as proposed by Dicke (Dicke, 1968).

MURAs can now be formed by mapping of the linear MURAs in exactly the same way as proposed before by Finger and Prince (Finger and Prince, 1985). Linear MURA can now be built in any length L that is a prime number and satisfies the condition $L = 4m + 1$, where $m = 1,2,3$ …. Similarly, linear MURAs use quadratic residue modulo L to establish locations of transparent and opaque elements in the coding array A. It was also shown that apertures can be formed in dimensions satisfying not only $p - q = 2$, but also $p - q = 0$ (Gottesman and Fenimore, 1989). The square option proved to be particularly popular due to a good balance between design complexity and the high resolution achieved.

3. Coded-aperture based X-ray imaging

Development of large scale X-ray imaging systems was mainly motivated by the space exploration missions SuperAGILE (Del Monte et al., 2007; Feroci et al., 2007), SWIFT (Gehrels et al., 2004), EXIST (Hong et al., 2004; Vadawale et al., 2005; Grindlay and Hong, 2004) and INTEGRAL (Bélanger et al., 2004). As a result, there exists a number of readily available X-ray imagers, where coded-aperture imaging is the dominant technique adopted. Different types of coded-aperture X-ray cameras and telescopes were implemented. Some systems utilise CdZnTe sensors for direct detection of the signals projected through the aperture (Gehrels et al., 2004; Hong et al., 2004; Tumerl et al., 1997). Other examples make use of sensitive silicon microstrip detectors (Del Monte et al., 2007; Feroci et al., 2007), where X-ray photons interact directly with the sensitive elements of the detector. Kinetic energy of photons is transformed into electrons, which can be processed by dedicated electronic circuitry.

A comprehensive account of coded-aperture applications in X-ray imaging for space exploration was presented by Caroli et al. (Caroli et al., 1987). A set of experiments was conducted to compare the coded-aperture based devices with other approaches. The advantages of using URA based coded masks, as opposed to fresnel pinhole or random masks, are clear when the angular resolution of the reconstruction is considered. Decreasing the hole size results in higher angular resolution – SNR is not affected as the increased number of holes can provide up to 50% aperture transparency. As the dimensions of the aperture elements are kept small, the overall size of the aperture may also be small and reduce the field of view (FOV) of the device. However, multiple devices can be built (in e.g. 2×2 configuration), which will compensate for FOV reduction at the cost of greater number of signals required to be processed on the output. This may in turn affect the detection speed as signals from the position sensitive detector require decoding to localise the source of radiation in the coded-aperture imaging systems.

A coded-aperture based X-ray camera, which utilises CCD as the position sensitive detector, was tested with a ^{241}Am source and the results confirmed the improvement in sensitivity when compared to a pinhole camera (Ivanov et al., 1999). In the experiment a device was built comprising a mask, CsI(Tl) scintillator, image intensifiers, CCD, lead shield and high voltage insulation. Different combinations of hole sizes and thicknesses were tested for two types of masks, namely single pinhole and coded-aperture mask based on HURA design. Sensitivity increase of up to four times was observed when images obtained by coded-aperture mask were contrasted with those generated by a single pinhole mask (Ivanov et al., 1999).

For comparison a 5 mm thick brass disk was used for both the HURA coded-aperture and the pinhole plate. Pinhole diameter was also kept the same for both tests at 2 mm. Images created using both techniques are presented in Fig. 2. The top four images shown in Fig. 2 are corresponding to the single hole plate case, and the bottom four images to the coded-aperture disk. It is clear that coded-aperture based reconstruction of the circular ^{241}Am source shows superior spatial resolution, when compared to the single hole plate.

4. Coded-aperture based gamma imaging

Since gamma-rays are released in a form of high energy photons, X-ray imaging methods can also be exploited for gamma-ray detection. Therefore, coded-apertures, as well as pinhole collimators have been implemented into scintillator based devices for gamma-ray detection and localisation. The primary application of coded-aperture based gamma-ray detectors in far-field high energy cameras for space exploration formed a basis for the study of near-field radiation detection in medicine and nuclear decommissioning. A very thorough investigation of coded-aperture approach as compared to pinhole camera collimator, for medical applications, was presented by Accorsi (Accorsi, 2001). Results of the study are presented in Table 1. These findings highlighted the advantages of employing coded-mask in place of a pinhole aperture when resolution and sensitivity are considered.

An often quoted disadvantage of coded-aperture approach is its limited FOV (Accorsi et al., 2001). Moreover, coded-aperture imagers are claimed to perform better than pinhole collimators only when point source localisation is performed. In spite of these potential weaknesses for large scale applications, recent research suggests that large horizontal FOV can be achieved by combining multiple coded-apertures into a single hexagonal device (Sun et al., 2015). In this particular case a system with 360° horizontal FOV presented angular resolution of average 3.5° when tested with standard calibration source of ^{137}Cs with energy of 662 keV. The system was also able to detect multiple sources in 360° FOV.

Detectors of such scale may sometimes be impractical for decommissioning applications as portability plays a key role during deployment. Therefore the overall dimensions are frequently decreased and, as a result, the FOV is reduced. Scanning collimator, for example RadScan, can be used to perform the analysis of greater area alleviating the problem of the limited FOV (Santo et al., 2006; Hughes et al., 2004). Exact location of radionuclides in nuclear decommissioning and environment characterisation applications is often unknown; hence the detection efficiency is of greater significance than the extended FOV.

A recent experiment performed by Gmar et al (Gmar et al., 2011). presents a strong correlation between the thickness of the mask used and the detection efficiency of a coded-aperture imaging system. During the study two MURA based masks were used – a rank 11, 4 mm thick mask and a rank 13, 2 mm thick mask. The rank number specifies the number of elements (pixels) comprising one side of a basic square MURA pattern, and coded-apertures are conventionally built by 2×2 arrangement of the basic pattern, following the cyclic permutation of rows and columns (Gottesman and Fenimore, 1989). Therefore, the total number of pixels for the rank 13 and the rank 11 aperture are 625 and 441 respectively. When both masks were tested with lower energy gamma-ray emitter (^{241}Am), the rank 13, 2 mm thick mask provided higher resolution than the rank 11, 4 mm thick aperture. However, when the system was exposed to relatively higher energy gamma sources (^{137}Cs and ^{60}Co), the rank 13, 2 mm thick mask performed distinctly inferior to the lower rank mask. In the latter case (^{60}Co) the configuration with rank 13, 2 mm thick aperture was found unable to detect the source (Gmar et al., 2011).

5. Neutron detection and coded-aperture imaging approach

The radioactive waste streams can contain neutron-emitting radioactive materials, hence localisation of neutron sources plays

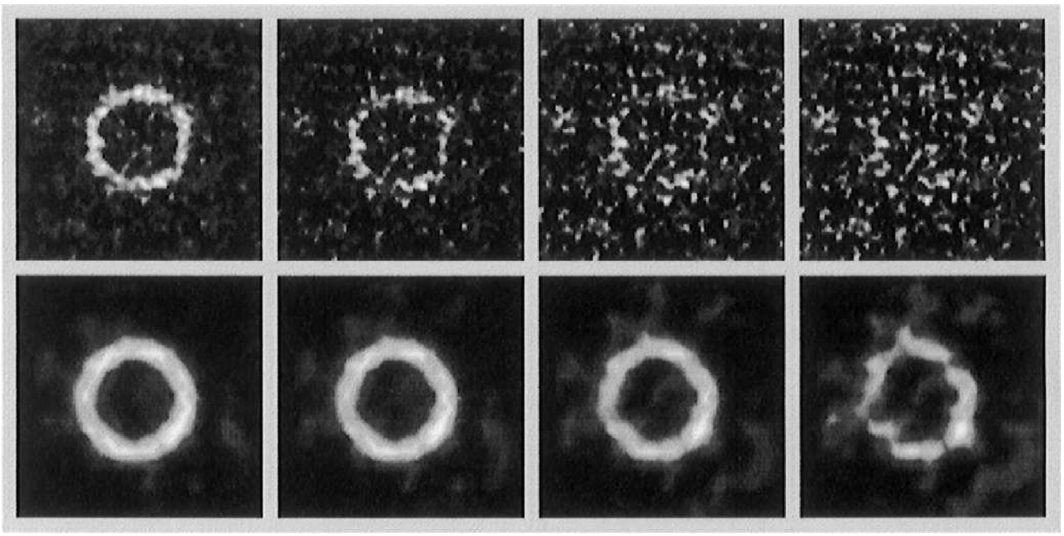

Fig. 2. Results of experiments carried out with a circular ^{241}Am source by Ivanov et al. (Ivanov et al., 1999). Detection time is equal to 8, 4, 2 and 1 of relative units (from left to right).

Table 1
Resolution and sensitivity comparison for collimator, pinhole and coded aperture with ^{99m}Tc used as gamma source (Accorsi, 2001).

Optics (^{99m}Tc)	Collimator		Pinhole	Coded aperture
	High sensitivity	Ultra-high resolution		
Hole diameter (mm)	2.54	1.16	4	1.11
Geometric resolution @ 10 cm (mm)	14.6	4.6	6.2	1.45
System resolution @ 10 cm (mm)	15.2	6.3	6.6	1.67
Sensitivity @ 10 cm (cpm/μCi)	1063	100	123	~ 10,000

an important part in nuclear decommissioning. It is of vital importance that personnel working on a nuclear site are also not exposed to neutron radiation. For many years, neutron detection systems were largely based on techniques involving ^{3}He as the primary detector, for example ^{3}He proportional counters were used extensively by security organisations to identify potential terrorist threats (Peerani et al., 2012). Despite its popularity and efficiency, an alternative system capable of neutron detection in real-time must be considered as ^{3}He supply has decreased sharply in the aftermath of September 2001 attacks.

Devices based on ^{3}He are preferred due to higher thermal neutron capture cross-section, in comparison to detection systems based on BF_3 gas-filled detectors (Knoll, 2010). Their absolute efficiency depends greatly on the thickness of the moderation material, which is used to slow down fast neutrons. Generally, detectors with the thicker moderation layer provide better response for higher energy neutron detection. However, if the moderator layer is too thick, lower energy neutrons may be captured by the moderator before reaching the sensitive part of the detector. Also, as the higher energy neutrons lose some of their energy before hitting the detector surface, the information about the neutron origin is lost. Consequently, the detection efficiency of the system is reduced (Knoll, 2010). Moreover, moderation thickness can limit the portability of the device, since significantly thicker moderation layer may be required for higher energy neutrons (Rees and Czirr, 2012).

Four alternative methods have been tested by Kouzes et al (Kouzes et al., 2010). identifying their absolute neutron efficiency and gamma-ray sensitivity. Each option was tested according to the specification of radiation portal monitoring (RPM) systems for national security in the United States. Only a set of three BF_3 tubes and a B-lined detector met the RPM absolute neutron detection efficiency requirement, as well as intrinsic gamma-ray efficiency requirement. Although BF_3 tubes proved to be effective for detection of slow neutrons, it would not be a feasible solution for fast neutron localisation due to significant efficiency reduction for higher energy neutrons (>100 eV) and moderation requirement in the same way as ^{3}He (Knoll, 2010).

Collimators coupled with B- and Gd-doped microchannel plates (MCP) present an interesting option for low energy neutrons. Neutrons are absorbed by B or Gd atoms inside the glass mixture plates, and electrons are emitted as a consequence of the absorption (Tremsin et al., 2005). Each of the electrons emitted is then multiplied inside an individual microchannel. This approach offers a very high spatial resolution, due to the dimensions of individual elements in the range of micrometers. As a result, the collimator size is also small. The weakness of the system lies in the requirement of stacking multiple MCPs to detect higher energy neutrons which are otherwise limited to thermal energy neutron detection.

An analogous method to Compton scattering for gamma-rays can be employed to image high energy neutrons. The neutron scatter camera method measures the energy of the recoil proton and time of flight (TOF) of the scattered neutron (Mascarenhas et al., 2006). Experiments performed showed that these two measurements are not sufficient to undoubtedly distinguish gamma photons from neutron events in mixed-field environment. It was essential to add a PSD module, so the signals can be reliably separated (Marleau et al., 2007).

A release of a neutron, following a nuclear reaction, is often accompanied by an emission of high energy gamma photons. Therefore, an efficient technique is required to distinguish between gamma-rays and neutron events in mixed radiation fields. Undoped organic liquid scintillators, such as EJ-301 and EJ-309, are regularly used to separate fast neutrons from gamma rays in mixed radiation

fields, due to their excellent PSD capabilities. The light pulses triggered by the neutron interactions, within the organic scintillator, decay more slowly as compared to those triggered by gamma ray interactions. The difference in the decay time is caused by greater energy loss rate for neutron than for gamma ray interactions within the scintillator (Gamage et al., 2011). Consequently, PSD can be performed to establish the type of the event detected. Various algorithms have been considered by the researchers in the time domain, as well as in the frequency domain (Gamage et al., 2011; Liu et al., 2010).

The aforementioned liquid scintillators (EJ-301 and EJ-309), were developed with capability of detecting fast neutrons, whereas they are not sensitive to thermal neutrons. They require doping with large thermal neutron capture cross-section isotopes to allow the detection of thermal neutrons. An example of such a detector is BC-523A, which is loaded with 4.4% of ^{10}B. As such, it presents greater detection efficiency when compared with the undoped EJ-309. In an experiment performed by Peerani et al (Peerani et al., 2012). both detectors were irradiated with ^{252}Cf and AmBe sources. Both detectors were 5 inch × 5 inch cylinders with a total detection volume of approximately 1600 cm^3. In each case detection efficiency was approximately 15% better for BC-523A than EJ-309. Moreover, PSD applied to organic liquid scintillators is insufficient to distinguish gamma photons from neutrons perfectly. A partial overlap between the gamma and neutron clouds is recorded suggesting an inevitable degree of misclassification of the events (Peerani et al., 2012). Recently developed plastic and crystal scintillators, such as EJ-299-33 (Eljen Technology, 2014) and stilbene (Inradoptics), promise a very good separation characteristics for neutrons and gamma-rays. However, the signals emitted by the plastic scintillators are faster compared to liquid scintillators making the application of PSD more challenging (Peerani et al., 2012).

Despite the challenges, PSD has been established as a standard method of separating neutron events from gamma-rays in radiation detectors based on organic scintillators. Development of fast ADCs and field programmable gate arrays (FPGAs) enabled PSD algorithms to be implemented reliably in the digital domain (Gamage et al., 2011; Hawkes et al., 2010). A well-established in the laboratory setting Charge Comparison Method (CCM) for example (Brooks, 1959), relies on the comparison of two time integrals of the detected pulse. The first integral is associated with the entire pulse, whereas the second one can be calculated as the area under the tail of the pulse. Hence, they are often described as the long and the short integral, respectively. The light pulse resulting from a gamma-ray photon interaction in the scintillator decays faster than the pulse corresponding to a neutron event. Consequently, the short integral is smaller for gamma-rays than for neutrons, when compared to the same magnitude long integral (Brooks, 1959; Adams and White, 1978). Alternatively, CCM can be defined as follows: the short integral as the peak of the pulse, and the long integral as the whole pulse. Regardless of the CCM definition, integration can be performed digitally by the summation of the areas under the pulse corresponding to each sample taken by the ADC.

5.1. Coded-aperture based approach

A large energy spectrum of neutron events complicates the employment of the coded-mask approach for neutron imaging. Therefore systems developed to date, focus on a specific energy range of neutrons. One of the implementations of the MURA based coded-aperture for thermal neutron detection was studied with a ^{3}He ionisation chamber (Vanier, 2004). High angular resolution obtained by coded-aperture based X- and gamma-ray imagers was maintained, when the same method was employed for thermal neutron localisation. Nevertheless the shortage of ^{3}He supply, as well as the limitations in portability of such a device makes the developments of ^{3}He based coded-aperture detection systems undesirable.

A fast neutron detector design based on the linear MURA using liquid scintillator EJ-301 revealed promising results when tested in security applications (Marleau et al., 2010). Both the mask as well as the detector plane were built using EJ-301 filled aluminium tubes (Marleau et al., 2009). This enabled the mask to scatter the fast neutrons rather than block them. As a result the neutrons detected in the mask were removed from the reconstructed image. The results showed high spatial resolution for two AmBe sources placed simultaneously in front of the aperture. The normally opaque elements of the coded-mask are replaced with neutron detectors. Consequently, neutron scattering occurs within the coded-mask, when the system is exposed to a fast neutron source. The scattered neutron will then disperse again (double scattering) when it causes another scattering event with the actual detector plane. Thus, the energy spectrum of the source can be determined by measuring the TOF between scatters. While the primary application of the system developed was fast neutron detection, it also exhibits potential for detecting gamma sources when PSD is applied. In an analogous test to the one performed for AmBe neutron source, a high energy gamma source ^{60}Co was placed 6.7 m away from the detector. The results presented support the claim of comparable detection efficiency for neutron and gamma-ray sources (Marleau et al., 2010).

Another implementation of a fast neutron and gamma-ray imaging system based on coded-aperture MURA pattern was developed at the U.S. Naval Research Laboratory (NRL) to support maritime security in the US (Woolf et al., 2012). The system tested comprises a square (13 × 13), 11.2 cm thick aperture made of Pb and high density polyethylene (HDPE) and an array of 30 liquid scintillation detectors (EJ-301). Each element of the aperture, as well as the detector is a 5.1 cm × 5.1 cm square. The detector array was placed 76 cm behind the coded-aperture. The system in this arrangement was tested with ^{252}Cf gamma/neutron source and ^{137}Cs gamma source placed 5.1 m away from the aperture plane. Since the lower energy threshold was set to >2.5 MeV neutron energy in each detector, there was no misclassifications recorded between gamma-ray and neutron events. An angular resolution of up to 4.6° was reported for the reconstructed images.

Further research conducted by the NRL led to a development of a large-scale, coded-aperture imager for fast neutrons (Woolf et al., 2015). In comparison to the work reported in the above paragraph, a 12 × 12 elements coded-aperture made of pure HDPE was built using pseudorandom pattern. EJ-301 scintillators were replaced with bigger EJ-309 detectors. The size of the individual detector was increased to 15 cm × 15 cm × 15 cm and the number of detectors to 32. The system was tested with two ^{252}Cf sources of different activities – 13 μCi (481 kBq) and 1.8 μCi (66.6 kBq) – located at various distances from the aperture. Similarly to the previous work, 4.5° angular resolution was reported in the reconstructed images. However, when the lower activity source was placed 26 m away from the aperture, it was not detected due to the high level of noise detected. Additional shielding around the detector array was necessary to improve the SNR and hence localise the lower activity source. Neutron and gamma PSD was implemented using digital CCM algorithm for each of 32 single channel PMTs.

MURA based coded-aperture fast neutron detection system was also tested for measurement of plutonium holdup at fuel cycle facilities (Hausladen et al., 46191). This system was a result of improvements to the previous work performed at Oak Ridge National

Laboratory (ORNL), which used liquid scintillators as sensitive detectors and utilised Pb shielding to block gamma-rays (Hausladen and Blackston; Hausladen et al., 1055983). The new system utilised modulating properties of HDPE to slow down the high energy neutrons, as the rank-11 MURA based aperture was built entirely from this material. In this experiment a new PSD capable plastic scintillator (EJ-299-34) was tested as a replacement to a fragile and susceptible to leaks liquid detector (EJ-309). The detector was built as an 8 × 8 array of individual plastic scintillator pixels with 1.35 × 1.35 × 5 cm^3 making the total volume of the detector to be 10.8 × 10.8 × 5 cm^3. The detector was positioned behind the 53.4 × 53.4 × 2.54 cm^3 coded-aperture pattern machined in an 81 × 81 × 2.54 cm^3 piece of HDPE. Multiple apertures can be joined together to increase the thickness of the HDPE if required. Several scenarios were tested with single and multiple ^{252}Cf sources placed in various location with the reference to the detection system. The main focus of the study was sensitivity rather than spatial resolution. The results suggest that the location of the neutron source in three dimensions can be inferred with a high level of accuracy (Hausladen et al., 46191). Nonetheless, the large scale of the system may present difficulties when attempting to incorporate such a system in nuclear decommissioning environment.

A different implementation of coded-masks to fast neutron localisation was presented by Brennan et al. (Brennan et al., 2015). In contrast to spatial modulation of a particle flux, normally used in coded-aperture imaging, time modulation of the particle flux was introduced. Time-encoded imaging (TEI) technique adapted in this study, relies on a small number of time-sensitive detectors, as opposed to position-sensitive detectors normally used in the coded-aperture imaging systems. Two time-sensitive detectors were built of two 1 inch diameter aluminium tubes filled with EJ-309 scintillator, coupled with two 2 inch diameter cylindrical PMT. The detectors were placed in the centre of a rotating circular mask made of HDPE. The mask had a 30% open fraction and the thickness chosen such that the fission neutrons were sufficiently moderated. The complete system was moved by a stepper motor which enabled the data from the motor encoder to be synchronised with the incidents detected by the PMTs. An angular resolution of 2° was achieved for two ^{252}Cf point sources after 12 h exposure time (Brennan et al., 2015). Due to the rotational operation of the system a 360° horizontal FOV can be realised. However, long exposure time required may prevent the employment of such systems where real or near real-time radiation detection is desired.

More recent attempts of utilising the coded-aperture approach for neutron detection also show promising results. If the coded-aperture is made of a neutron absorbing material, its thickness affects the overall performance of the detector. Recently performed Monte Carlo simulations used an 8 cm thick MURA based coded-aperture model (made of ^{10}B, ^{113}Cd and ^{157}Gd), EJ-426 – a thermal neutron scintillator – and ^{241}AmBe as the neutron source. The results present high spatial resolution for the neutron source located near the central point of the aperture. However, a decrease in spatial resolution is observed when the source is placed nearer the edges of the aperture. The decrease is caused by a greater number of neutrons being absorbed by the shielding implemented around the edges of the coded-aperture. Since fewer neutrons reach the detector surface, the accuracy of the source reconstruction decreases (Hayes and Gamage, 2013).

Despite the high angular resolution achieved across the coded-aperture based neutron imagers presented in this section, their adaptation for nuclear decommissioning remains to be demonstrated. None of the systems described performs neutron localisation in real-time. Moreover, the large scale systems (Hausladen et al., 46191; Marleau et al., 2007; Brennan et al., 2015) would be difficult to deploy or maneuver within a nuclear decommissioning environment. They would be impractical in the environment where portability of radiation imaging systems is crucial.

6. Potential improvements to coded-aperture based neutron imaging

The currently employed techniques for neutron imaging do not offer sufficient sensitivity across the energy spectrum between thermal and fast neutrons (up to 15 MeV). Existing research suggests adding moderation materials or building apertures of greater thicknesses to solve the problem. These solutions may substantially increase the weight and limit the portability of the complete imaging system.

Portable, real-time neutron imaging will be of great benefit to nuclear decommissioning and security applications. In this paper, authors simulated a coded-aperture model considering the practicality of such a device. The shape and the dimensions of the aperture are also chosen such that a scintillator and a position sensitive photo multiplier tube (PSPMT) can be matched. Since an organic scintillating material which is sensitive to a range of neutron energies between thermal and fast (up to 15 MeV) is not available, focus was placed on developing a system suitable for the digital PSD implementation. Modern organic liquid scintillators offer discrimination between neutron and gamma incidents down to approximately 40 keVee, which corresponds to 450 keV energy neutrons (Yong-Hao et al., 2014; Balmer et al., 2015). Improvements into methods of growing single stilbene crystals led to a development of a scintillator, which claims better PSD for lower energy neutrons than previously mentioned EJ-309 liquid scintillator (Gerling et al., 2014). Hence, the prospect of utilising the stilbene scintillator will be explored. The system could then be paired with a multi-channel, FPGA based signal processing electronic circuitry, making real-time detection, localisation and discrimination of neutron and gamma sources in a mixed radiation field possible.

6.1. Design of MURA based coded aperture

The model created in this work comprises a square rank 7 coded-aperture with 169 elements, a scintillator and a neutron source. The coded-aperture was designed using original MURA algorithm (Gottesman and Fenimore, 1989). The design of the coded-aperture based system involves construction of both an encoding and a decoding array. The encoding array A is placed in front of a source of radiation S resulting in an encoded image being projected on the detector surface D. Considering the practicality of the simulated system, a 13 × 13 aperture – the encoding array A – was designed through a 2 × 2 arrangement of the basic rank 7 pattern. Location of opaque and transparent elements in the encoding array A was determined by following equations (1) and (2) (Gottesman and Fenimore, 1989).

$$A_{ij} = \begin{cases} 0 & \text{if } i = 1, \\ 1 & \text{if } j = 0, i \neq 0, \\ 1 & \text{if } C_i C_j = +1, \\ 0 & \text{otherwise}, \end{cases} \tag{1}$$

where

$$C_i, C_j = \begin{cases} +1 & \text{if } i \text{ is a quadratic residue modulo L}, \\ -1 & \text{otherwise}. \end{cases} \tag{2}$$

The quadratic residue modulo L calculation stems from the number theory and identifies which elements in each row C_i and each column C_j should be open (+1) or closed (−1). As the case $L = 0$ is normally excluded from the lists, quadratic residue lists

typically range from *1* to *L−1* (Hardy and Wright, 1979); from 1 to 6 for the system considered in this work.

Equation (1) is then applied to include the row and column when i and j are equal to zero. The resulting encoding array A is obtained by simply replacing $+1$ terms with *1* and -1 terms with *0*. In accordance with equation (1), the row with i equal to zero contains all zeros, whereas the column with j equal to zero contains all ones apart from the case when i is zero. Such an aperture can be easily rearranged into a symmetrical form by a cyclic permutation of rows and columns (Gottesman and Fenimore, 1989). The basic array in this form can be simply made into 2×2 version as presented in Fig. 3.

$$G_{ij} = \begin{cases} +1 & \text{if } i+j=0; \\ +1 & \text{if } A_{ij}=1, (i+j\neq 0); \\ -1 & \text{if } A_{ij}=0, (i+j\neq 0); \end{cases} \quad (3)$$

In order to decode the image projected by the aperture, equation (3) is applied to the array A resulting in the decoding array G. In this case all *0* terms are changed to -1 and all *1* terms to $+1$ except for the situation when the *0* term for $i,j = 0$ is replaced with $+1$. In the 2×2 arrangement of the basic array, it is the middle element that changes its value in comparison to the encoding array A (Gottesman and Fenimore, 1989).

The reconstructed image R is obtained by applying the convolution theorem to the image projected on the detection plane D and the decoding array G as presented in equation (4). The detection plane array D was obtained by running a simulation in MCNPX (Booth et al., 2005).

$$R = D*G; \quad (4)$$

7. MCNPX modelling and simulation

As creation of complicated geometry models in MCNPX can be troublesome and error-prone, MCAM CAD-based software was used for the design of the aperture and detector plane (Wu et al., 2015). Models can be built in 3D and converted to commonly used radiation transport codes e.g. MCNP, Geant4. The model of the aperture created in MCAM is shown in Fig. 4. It was created by closely following the equations presented in the previous subsection.

^{113}Cd and naturally occurring W were tested as potential materials for the coded-mask considering their neutron modulating and reflecting properties (Gamage et al., 2012). ^{113}Cd was chosen due to its relatively high thermal neutron absorption cross-section (26,719 b). High atomic number of natural W, and its low thermal neutron absorption cross-section (23.86 b) provide marginal moderation of neutrons but adequate reflection for high energy neutrons, due to its high density (19.3 g/cm^3). Moreover, mean free path was calculated for each material for thermal and 15 MeV neutrons (maximum neutron energy of ^{252}Cf as specified in (International Organization for Standardization, 2001)). Results presented in Table 2 support the assumption that ^{113}Cd is a better choice for thermal neutron absorption than natural W. However, high density of the natural W is reflected in the comparison between the mean free path values for the two materials at 15 MeV. In both cases, an increase in detection sensitivity is to be expected when the aperture thickness is increased. Therefore, aperture models of two thicknesses were tested −10 mm and 25 mm. Each square element of the aperture was set to 5 mm × 5 mm. The size of each detector element is identical to the thinner aperture in terms of area as well as thickness of a single element.

Commercially available liquid scintillators, for instance EJ-301, present good PSD characteristics. But their implementation in systems targeted for nuclear decommissioning can be hindered by some of their properties: for example, EJ-301 consists of highly toxic, flammable and volatile aromatics. Recently developed plastic scintillators have proven to achieve similar results to organic liquid scintillators with regard to PSD (Zaitseva et al., 2012). As these detectors are not manufactured from dangerous substances, they present a potential for use in neutron detection application in nuclear decommissioning.

Recent research into methods of obtaining single stilbene

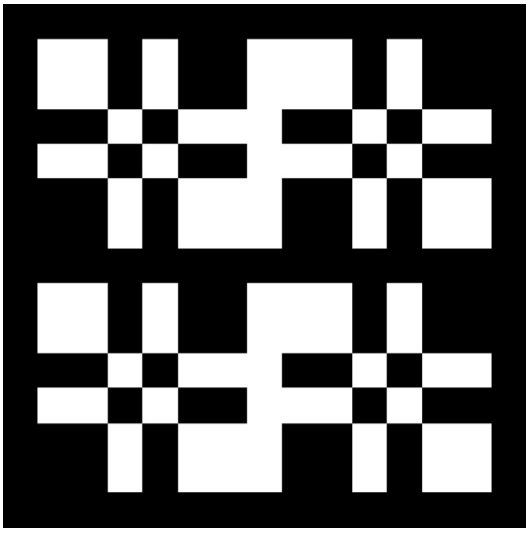

Fig. 3. Rank 7 coded-aperture. Transparent and opaque elements are presented in white and black, respectively. With 84 transparent and 85 opaque elements, the modelled aperture yields 49.7% transparency. A frame of 5 mm was added around the 13 × 13 aperture to represent clear boundaries.

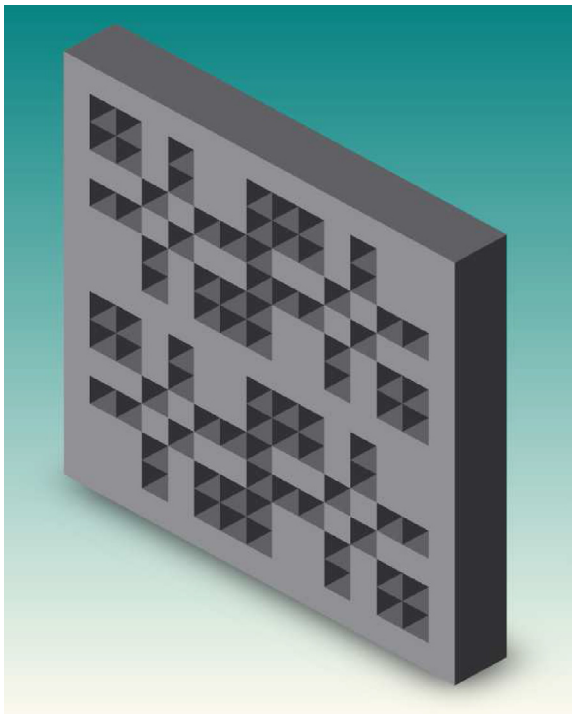

Fig. 4. Aperture with the 5 mm frame constructed in MCAM.

Table 2
Neutron mean free path calculation results for ^{113}Cd and Natural W based on ENDF/B-VII.1 library from (Soppera and Dupont, 2012).

Material	Neutron mean free path (cm)	
	Thermal	15 MeV
^{113}Cd	8.112×10^{-4}	4.78
Natural W	0.664	2.954

crystals suggests that their light output can be two times higher than that of commonly used liquid scintillator (EJ-309) (Knoll, 2010; Zaitseva et al., 2015). Furthermore, a comparison performed between EJ-309 and stilbene crystal scintillators shows that stilbene has superior PSD and energy resolution (Gerling et al., 2014). These developments in stilbene manufacture made it a viable candidate for the work undertaken. Therefore a stilbene crystal scintillator (C_{14} H_{12}) with density of (1.15 g/cm^3) was modelled in the MCNPX environment (Inradoptics). According to the technical data sheet, the crystal offers excellent neutron gamma separation, while being non-hygroscopic, non-flammable and non-hazardous (Inradoptics); features of great importance in industrial applications.

As the primary interest of this work lies in localisation of neutron sources, ^{252}Cf was modelled as the radiation source. It was defined in the MCNPX code based on the characteristics specified in the BS ISO 8529-1:2001 standard (International Organization for Standardization, 2001). ^{252}Cf spontaneous fission source releases several fast neutrons as a result of each fission event (Knoll, 2010), which makes it a viable choice for the requirements of the work described in this paper.

MCNPX geometries were set up with the ^{252}Cf point source, represented as a red sphere in Fig. 5, located either 5 cm or 10 cm away from the aperture. The coded-aperture and the detector plane - shown in grey and yellow in Fig. 5, respectively - were arranged to be 10 cm apart. The midpoint of the aperture was located at the origin of the geometry regardless of its thickness. As a result, the coordinates of the source in space were changing, as the thickness of the aperture was altered.

A pulse height tally was recorded for each detector cell. The pulse height tally (F8) was chosen as the data recorded offers the closest representation of a physical detector cell (Booth et al., 2005). Special treatment of the pulse height tally was utilised (FT8 CAP), which transforms it to a neutron capture tally (Pelowitz, 2011).

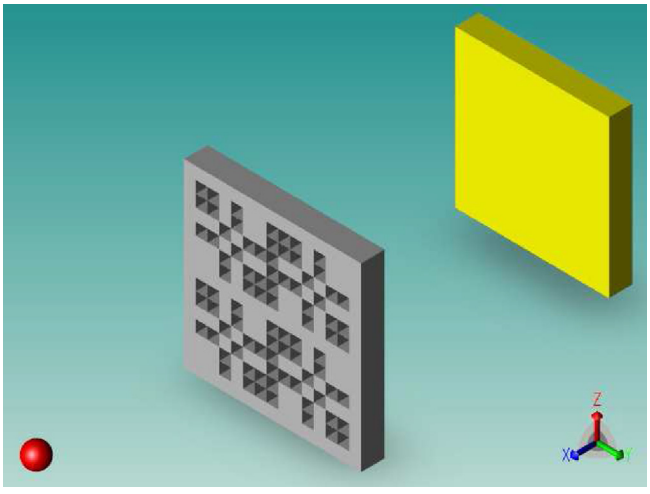

Fig. 5. 3D image of the complete MCPNX geometry.

Once MCNPX completed each simulation, number of neutrons captured within each detector cell were read through a MATLAB script and then stored as a 13 × 13 array. The array obtained is equivalent to the detector plane array *D* described in section 6.1. Using MATLAB, the detector plane array *D* was convoluted with the decoding array *G* and the resultant was utilised to find the reconstructed array *R*.

7.1. Simulation results

For each simulation scenario cell particle activity table – table 126 in MCNPX output file - was analysed and compared for the two aperture materials modelled. Across all arrangements tested, number of neutron collisions in the aperture was on average 40% higher in the natural W than in ^{113}Cd. Additionally, average neutron mean free path was greater (approx. 3.78 cm) for ^{113}Cd than for W (approx. 2.32 cm). These results are comparable with the values presented in Table 2., given the theoretical analysis was performed for the maximum energy of the specified source rather than the average.

Detection errors were calculated based on the results obtained. The errors presented in Tables 3 and 4 took into account the difference between the actual source position and the location obtained through the reconstruction process described. The results are presented as 2D images with a scale between −3 and +3 cm in Y and Z directions. Given the rank of the aperture and the dimensions of the detector simulated, the centre of each cell is located every 0.5 cm. Hence the maximum error (100%) in one direction is associated with the situation, when a hot-spot is detected 6 cells away from the actual location of the source. For example Fig. 6(b), presents the reconstructed source at Y = 3 cm i.e. 6 cells away from the actual source in Y direction - maximum error 100%. In the Z direction the difference is only 1/6 cells (Z = 0.5 cm) - approximate error 16.67%. Using trigonometry the resultant error can be calculated to be 25.32% (accounting for the fact that only one quarter of the whole graph is considered).

In the first modelled set-up, the source was located at (5.5 cm, 0.0 cm, 0.0 cm) with the front of the 10 mm thick aperture, exactly 5 cm behind. Images of the reconstructed arrays *R* were plotted for each simulated scenario. Fig. 6(a) and (b) present plots of the filtered neutron capture results for ^{113}Cd and natural W, respectively. It can be observed that both materials provide low detection sensitivity, when the source is located only 5 cm away from the aperture and neutron capture tallies are considered. The following two plots – Fig. 6(c) and (d) – represent the reconstruction of the sources for the aperture of 25 mm thickness with the neutron source located 5 cm away. Although the detection accuracy increases marginally in the case of natural W when the aperture thickness is increased, it is not sufficient to provide reliable localisation data.

Results of the simulation for the source located at the distance of 10 cm from the aperture front present a significant improvement in detection sensitivity, when compared to the previously discussed case. Regardless of the thickness ^{113}Cd aperture provides an ideal reconstruction of the source. The improvement for the mask made of natural W is not as prominent as in the case of ^{113}Cd. It should

Table 3
Detection error for the distance of 5 cm between the source and the aperture.

Material	Detection error (%)	
	10 mm thick	25 mm thick
^{113}Cd	18.45	18.45
Natural W	25.32	21.13

Table 4
Detection error for the distance of 10 cm between the source and the aperture.

Material	Detection error (%)	
	10 mm thick	25 mm thick
^{113}Cd	0.00	0.00
Natural W	18.34	13.12

also be noted that a weighted error calculation was applied for all the images presented. Hence, the detection error is greater for 10 mm thick W mask, as contrasted with the 25 mm thick W mask; multiple hot-spots suggest lower confidence in the results obtained. The reason for image splitting can be associated with the neutron reflective properties of natural W. As the aperture is placed farther away from the source, a higher number of particles can be reflected through the internal surfaces of the aperture's open elements. These in turn lead to false neutron events being detected within scintillator cells.

Since the main focus of this study was to assess a workable neutron localisation solution for nuclear decommissioning an isotropic ^{252}Cf source was used. It was found that ^{113}Cd aperture absorbed lower number of neutrons than natural W, which supports the calculated and achieved neutron mean free path values for each material. In both cases the statistical uncertainty of the results did not exceed 0.01% for the neutron capture tally. The detectors response in the relevant energy ranges did not exceed the statistical uncertainty of 0.05%. This level of statistical accuracy was achieved with 10^8 particle histories simulated.

The modelled stilbene scintillator performed well in the simulated environment, despite its small thickness (1 cm), which makes it a possible solution for practical implementation of the system. Moreover, initial results suggest that even with a relatively large element size (5 mm × 5 mm) and small thickness of 10 mm, ^{113}Cd coded-aperture can achieve good detection sensitivity as shown in Fig. 7(a) and (c). It should also be noted that with doubling of the distance between the aperture and the neutron source, an improvement in detection sensitivity was observed. The importance of this is that neutron localisation from a distance would be of great benefit for nuclear decommissioning applications, as access to the areas of nuclear power plants requiring characterisation is often limited.

8. Discussion

Existing coded-aperture imaging systems have been reviewed and potential improvements for a practical coded-aperture based neutron imaging system have been discussed and simulated. Scintillator based coded-aperture radiation imaging has been previously well documented by researchers with reference to X- and gamma-ray detection. Coded-aperture neutron imaging systems have shown encouraging results for fast neutron detection in security applications, as well as in nuclear material instrumentation. Neutron detection and localisation in nuclear decommissioning, on the other hand, relies largely on commercially available collimator

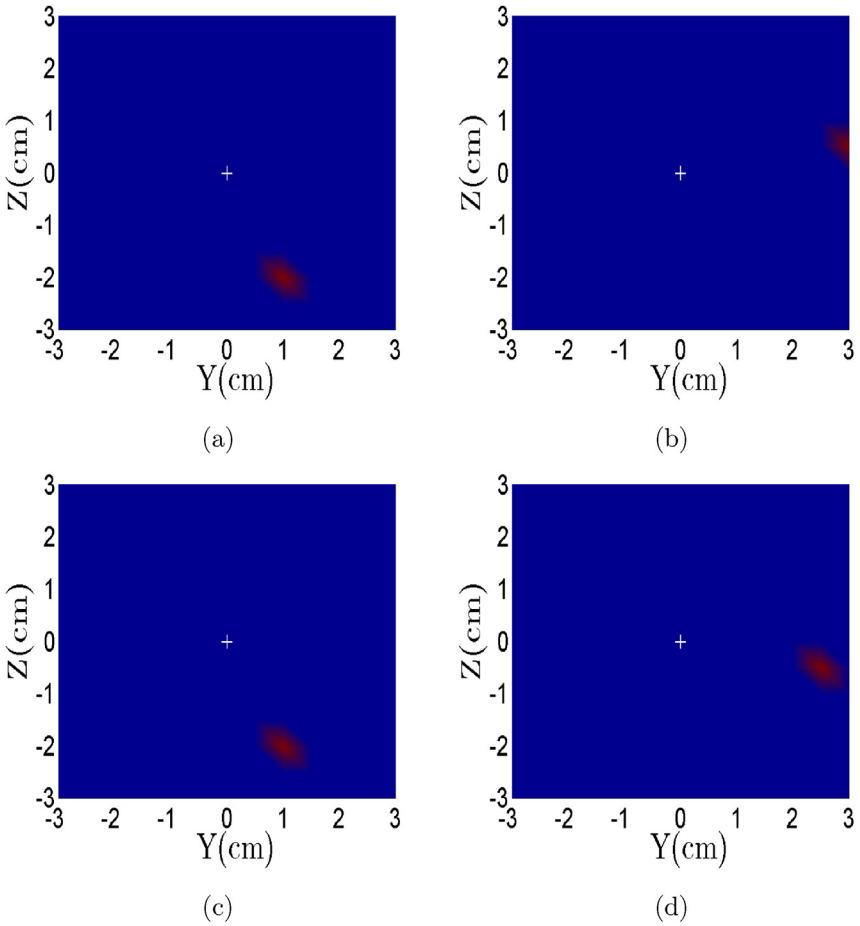

Fig. 6. MATLAB plots of MCNPX simulation results with ^{252}Cf source located 5 cm away from the aperture: (a) ^{113}Cd aperture, thickness – 10 mm (b) W aperture, thickness – 10 mm, (c) ^{113}Cd aperture, thickness – 25 mm and (d) W aperture, thickness – 25 mm. White cross marks the actual location of the source.

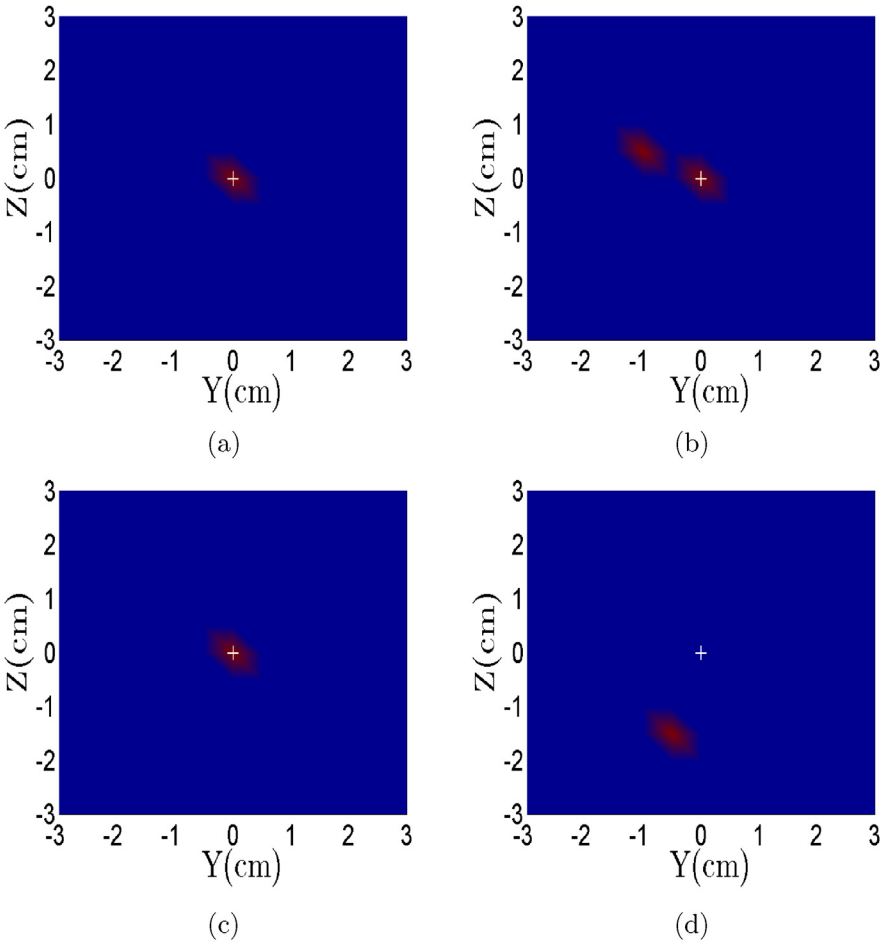

Fig. 7. MATLAB plots of MCNPX simulation results with ^{252}Cf source located 10 cm away from the aperture: (a) ^{113}Cd aperture, thickness – 10 mm (b) W aperture, thickness – 10 mm, (c) ^{113}Cd aperture, thickness – 25 mm and (d) W aperture, thickness – 25 mm. White cross marks the actual location of the source.

based pinhole detectors. Many of these systems employ liquid scintillation detectors, which are not favourable in sensitive decommissioning environment, due to their hazardous properties. In this study, an organic stilbene crystal scintillator has been identified, which claims excellent PSD, and provided promising results in the fast neutron environment modelled. In contrast to liquid scintillators, it is not hazardous, easy to transport and not susceptible to leaks. Furthermore, the results obtained from an MCNPX simulation also suggest that using high density material for the mask enables it to reliably stop fast neutrons from reaching the scintillator through the opaque elements of the mask, without increasing its thickness to impractical dimensions.

The theoretical model proposed holds potential for a portable coded-aperture neutron detection system if paired with a commercially available PSPMT, such as Hamamatsu H9500. It is a square 256 channel PSPMT with pixel size of 2.8 mm × 2.8 mm. The size of a single coded-aperture element can be matched to that of the PMT pixel increasing the overall resolution of the system. As the location of the interaction in the scintillator can be extracted via readout electronic system, the detection sensitivity could also be potentially increased. However, in order to reliably distinguish neutron from gamma interactions within organic scintillator, not only the interaction location but also the shape of the pulse must be retrieved. Hence, a bespoke readout electronic system for the PSPMT would be required. Pulses extracted from the PSPMT would necessitate digitisation using high sampling rate ADCs before being processed on a fast FPGA chip (up to 500 MHz) to perform digital PSD. With a correctly characterised scintillator, real-time mixed field characterisation could be achieved.

The modelling work completed, proposes one of the implementations of the scintillator based coded-aperture neutron imaging systems. In comparison to the coded-aperture neutron imaging systems reviewed, the model proposed in this paper is a relatively small scale system. It aims to present an adaptation of the proven advantages of the larger coded aperture imaging systems for neutron localisation in nuclear decommissioning, where portability and detection efficiency play vital roles. Hence, the system is intended to perform initial scanning of a larger area from a distance of several meters and then gradually focus on the specific location of the radioactive source. Alternatively, multiple modules can be arranged into square arrays avoiding the need for initial scanning of larger areas.

As scintillator based coded-aperture neutron imagers are continuously being explored and improved, owing to technological advancement, coded-aperture based neutron imagers can be adapted in new application fields, such as nuclear decommissioning. Hence, a careful selection of hardware elements, a novel design approach, as well as innovative digitised PSD implementation will play a key role in the performance of an imaging system suitable for this application.

Acknowledgements

The authors would like to acknowledge the funding support from EPSRC (grant number EP/M507891/1) via Faculty of Science and Technology, Lancaster University, UK and Sellafield Ltd., UK. We also acknowledge the help and advise of Mr. Matthew Balmer at Lancaster University, UK.

References

Ables, J.G., 1968. Fourier transform photography: a new method for X-ray astronomy. Proc. Astron. Soc. Aust. 1, 172–173.

Accorsi, R., 2001. Design of Near-field Coded Aperture Cameras for High-resolution Medical and Industrial Gamma-Ray Imaging. Ph.D. thesis. Massachusetts Institute of Technology. Dept. of Nuclear Engineering. http://hdl.handle.net/1721.1/8684.

Accorsi, R., Gasparini, F., Lanza, R., 2001. A coded aperture for high-resolution nuclear medicine planar imaging with a conventional Anger camera: experimental results. IEEE Trans. Nucl. Sci. 48 (6), 2411–2417. http://dx.doi.org/10.1109/23.983251.

Adams, J., White, G., 1978. A versatile pulse shape discriminator for charged particle separation and its application to fast neutron time-of-flight spectroscopy. Nucl. Instrum. Methods 156 (3), 459–476. http://dx.doi.org/10.1016/0029-554X(78)90746-2.

Alnafea, M., Wells, K., Spyrou, N.M., Saripan, M.I., Guy, M., Hinton, P., 2006. Preliminary results from a Monte Carlo study of breast tumour imaging with low-energy high-resolution collimator and a modified uniformly-redundant array-coded aperture. Nucl. Instrum. Methods Phys. Res. Sect. A Accel. Spectrom. Detect. Assoc. Equip. 563 (1), 146–149. http://dx.doi.org/10.1016/j.nima.2006.01.124.

Alnafea, M., Wells, K., Spyrou, N., Guy, M., 2007. Preliminary Monte Carlo study of coded aperture imaging with a CZT gamma camera system for scinti-mammography. Nucl. Instrum. Methods Phys. Res. Sect. A Accel. Spectrom. Detect. Assoc. Equip. 573 (1–2), 122–125. http://dx.doi.org/10.1016/j.nima.2006.11.007.

P. Hausladen, J. Newby, F. Liang, M. Blackston, The Deployable Fast-Neutron Coded-Aperture Imager : Demonstration of Locating One or More Sources in Three Dimensions. URL http://info.ornl.gov/sites/publications/files/Pub46191.pdf.

P. Hausladen, M. Blackston, Passive and Active Fast-Neutron Imaging in Support of AFCI Safeguards Campaign Prepared by, Energy (August). doi:10.2172/978279.

P. Hausladen, M. Blackston, E. Brubaker, D. Chichester, P. Marleau, R. Newby, Fast-Neutron Coded-Aperture Imaging of Special Nuclear Material Configurations. URL http://digital.library.unt.edu/ark:/67531/metadc832970/m2/1/high_res_d/1055983.pdf.

Baek, C.-H., An, S.J., Kim, H.-I., Kwak, S.-W., Chung, Y.H., 2013. Development of a pinhole gamma camera for environmental monitoring. Radiat. Meas. 59, 114–118. http://dx.doi.org/10.1016/j.radmeas.2013.06.004.

Balmer, M., Gamage, K., Taylor, G., 2015. Neutron assay in mixed radiation fields with a ^{6}Li-loaded plastic scintillator. J. Instrum. 10 (08), P08012. http://dx.doi.org/10.1088/1748-0221/10/08/P08012.

Bélanger, G., Goldwurm, A., Goldoni, P., Paul, J., Terrier, R., Falanga, M., Ubertini, P., Bazzano, A., Del Santo, M., Winkler, C., Parmar, A.N., Kuulkers, E., Ebisawa, K., Roques, J.P., Lund, N., Melia, F., 2004. Detection of hard x-ray emission from the galactic nuclear region with INTEGRAL. Astrophysical J. 601, L163–L166. http://dx.doi.org/10.1086/381738.

Booth, T.E., Grady Hughes, H., Zukaitis, A., Brown, F.B., Mosteller, R.D., Boggs, M., Bull, J.S., Prael, R.E., Martz, R., Forster, R.A., Sood, A., Goorley, J.T., Sweezy, J.E., 2005. MCNP - a General Monte Carlo N-particle Transport Code, Version 5, User Manual.

Brennan, J., Brubaker, E., Gerling, M., Marleau, P., McMillan, K., Nowack, A., Galloudec, N.R.-L., Sweany, M., 2015. Demonstration of two-dimensional time-encoded imaging of fast neutrons. Nucl. Instrum. Methods Phys. Res. Sect. A Accel. Spectrom. Detect. Assoc. Equip. 802, 76–81. http://dx.doi.org/10.1016/j.nima.2015.08.076.

Brooks, F., 1959. A scintillation counter with neutron and gamma-ray discriminators. Nucl. Instrum. Methods 4 (3), 151–163. http://dx.doi.org/10.1016/0029-554X(59)90067-9.

Calabro, D., Wolf, J.K., 1967. On the synthesis of two-dimensional arrays with desirable correlation properties. Inf. Control 11 (5–6), 537–560. http://dx.doi.org/10.1016/S0019-9958(67)90755-3.

Caroli, E., Stephen, J.B., Di Cocco, G., Natalucci, L., Spizzichino, A., 1987. Coded aperture imaging in X- and gamma-ray astronomy. Space Sci. Rev. 45, 349–403. http://dx.doi.org/10.1007/BF00171998.

Cattle, B.A., Fellerman, A.S., West, R.M., 2004. On the detection of solid deposits using gamma ray emission tomography with limited data. Meas. Sci. Technol. 15 (7), 1429–1439. http://dx.doi.org/10.1088/0957-0233/15/7/027.

Cook, W.R., Finger, M., Prince, T.A., Stone, E.C., 1984. Gamma-ray imaging with a rotating hexagonal uniformly redundant array. IEEE Trans. Nucl. Sci. NS-31 (1), 771–775.

Damato, A.L., Horn, B.K.P., Lanza, R.C., 2007. Coded source imaging for neutrons and X-rays. IEEE Nucl. Sci. Symposium Conf. Rec. 1, 199–203. http://dx.doi.org/10.1109/NSSMIC.2006.356138.

Del Monte, E., Costa, E., Di Persio, G., Donnarumma, I., Evangelista, Y., Feroci, M., Frutti, M., Lapshov, I., Lazzarotto, F., Mastropietro, M., Morelli, E., Pacciani, L., Porrovecchio, G., Rapisarda, M., Rubini, A., Soffitta, P., Tavani, M., Argan, A., 2007. An X-ray imager based on silicon microstrip detector and coded mask. Nucl. Instrum. Methods Phys. Res. Sect. A Accel. Spectrom. Detect. Assoc. Equip. 576 (1), 191–193. http://dx.doi.org/10.1016/j.nima.2007.01.150.

Dicke, R.H., 1968. Scatter-hole cameras for x-rays and gamma rays. Astrophysical J. 153, 101–106. http://dx.doi.org/10.1086/180230.

Eljen Technology, April 2014. EJ-299–33A PSD Plastic Scintillator, Data Sheet. http://www.eljentechnology.com/index.php/products/plastic-scintillators/114-ej-299-33.

Faust, A.A., Rothschild, R.E., Leblanc, P., McFee, J.E., 2009. Development of a coded aperture X-Ray backscatter imager for explosive device detection. IEEE Trans. Nucl. Sci. 56 (1), 299–307. http://dx.doi.org/10.1109/TNS.2008.2009537.

Fenimore, E.E., Cannon, T.M., 1978. Coded aperture imaging with uniformly redundant arrays. Appl. Opt. 17 (3), 337–347. http://dx.doi.org/10.1364/AO.17.000337.

Feroci, M., Costa, E., Soffitta, P., Del Monte, E., Di Persio, G., Donnarumma, I., Evangelista, Y., Frutti, M., Lapshov, I., Lazzarotto, F., Mastropietro, M., Morelli, E., Pacciani, L., Porrovecchio, G., Rapisarda, M., Rubini, a., Tavani, M., Argan, a., 2007. SuperAGILE: the hard X-ray imager for the AGILE space mission. Nucl. Instrum. Methods Phys. Res. Sect. A Accel. Spectrom. Detect. Assoc. Equip. 581 (3), 728–754. http://dx.doi.org/10.1016/j.nima.2007.07.147.

Finger, M.H., Prince, T.A., 1985. Hexagonal uniformly redundant arrays for coded-aperture imaging. Int. Cosm. Ray Conf. 3, 295–298.

Gal, O., Dessus, B., Jean, F., Laine, F., Leveque, C., 2000. Functioning of the cartogam portable gamma camera in a photon counting mode. In: Nuclear Science Symposium Conference Record. IEEE. http://dx.doi.org/10.1109/NSSMIC.2000.949225. Vol. 1, 2000, pp. 6/308–6/312 vol. 1.

Gal, O., Dessus, B., Jean, F., Laine, F., Leveque, C., 2001. Operation of the cartogam portable gamma camera in a photon-counting mode. IEEE Trans. Nucl. Sci. 48 (4), 1198–1204. http://dx.doi.org/10.1109/23.958750.

Gamage, K., Joyce, M., Hawkes, N., 2011. A comparison of four different digital algorithms for pulse-shape discrimination in fast scintillators. Nucl. Instrum. Methods Phys. Res. Sect. A Accel. Spectrom. Detect. Assoc. Equip. 642 (1), 78–83. http://dx.doi.org/10.1016/j.nima.2011.03.065.

Gamage, K.A.A., Joyce, M.J., Taylor, G.C., 2012. A comparison of collimator geometries for imaging mixed radiation fields with fast liquid organic scintillators. IEEE Trans. Nucl. Sci. 59 (4), 1432–1437. http://dx.doi.org/10.1109/TNS.2012.2185710.

Gehrels, N., Chincarini, G., Giommi, P., Mason, K.O., Nousek, J.A., Wells, A.A., White, N.E., Barthelmy, S.D., Burrows, D.N., Cominsky, L.R., Hurley, K.C., Marshall, F.E., Meszaros, P., Roming, P.W.A., Angelini, L., Barbier, L.M., Belloni, T., Campana, S., Caraveo, P.A., Chester, M.M., Citterio, O., Cline, T.L., Cropper, M.S., Cummings, J.R., Dean, A.J., Feigelson, E.D., Fenimore, E.E., Frail, D.A., Fruchter, A.S., Garmire, G.P., Gendreau, K., Ghisellini, G., Greiner, J., Hill, J.E., Hunsberger, S.D., Krimm, H.A., Kulkarni, S.R., Kumar, P., Lebrun, F., Lloyd Ronning, N.M., Markwardt, C.B., Mattson, B.J., Mushotzky, R.F., Norris, J.P., Osborne, J., Paczynski, B., Palmer, D.M., Park, H., Parsons, A.M., Paul, J., Rees, M.J., Reynolds, C.S., Rhoads, J.E., Sasseen, T.P., Schaefer, B.E., Short, A.T., Smale, A.P., Smith, I.A., Stella, L., Tagliaferri, G., Takahashi, T., Tashiro, M., Townsley, L.K., Tueller, J., Turner, M.J.L., Vietri, M., Voges, W., Ward, M.J., Willingale, R., Zerbi, F.M., Zhang, W.W., 2004. The swift gamma ray burst mission. Astrophysical J. 611 (2), 1005–1020. http://dx.doi.org/10.1086/422091.

Gerling, M., Marleau, P., Goldsmith, J., 2014. Comparison of Stilbene Neutron Detection Performance to EJ-309. http://prod.sandia.gov/techlib/access-control.cgi/2014/1419914r.pdf.

Gmar, M., Agelou, M., Carrel, F., Schoepff, V., 2011. GAMPIX: a new generation of gamma camera. Nucl. Instrum. Methods Phys. Res. Sect. A Accel. Spectrom. Detect. Assoc. Equip. 652 (1), 638–640. http://dx.doi.org/10.1016/j.nima.2010.09.003.

Goldwurm, A., Byard, K., Dean, A.J., Hall, C.J., Harding, J.S.J., 1990. Laboratory images with HURA coded apertures. Astronomy Astrophysics 227, 640–648.

Gottesman, S.R., Fenimore, E.E., 1989. New family of binary arrays for coded aperture imaging. Appl. Opt. 28 (20), 4344–4352. http://dx.doi.org/10.1364/AO.28.004344.

Gottesman, S.R., Schneid, E.J., 1986. PNP - a new class of coded aperture arrays. IEEE Trans. Nucl. Sci. 33 (1), 745–749.

Grindlay, J.E., Hong, J., 2004. Optimizing wide-field coded aperture imaging: radial mask holes and scanning. In: Proceedings SPIE, Optics for EUV, X-Ray, and Gamma-Ray Astronomy, vol. 5168, pp. 402–410. http://dx.doi.org/10.1117/12.506260.

Hardy, G.H., Wright, E.M., 1979. An Introduction to the Theory of Numbers, fifth ed. Oxford University Press.

Hawkes, N.P., Gamage, K.A.A., Taylor, G.C., 2010. Digital approaches to field neutron spectrometry. Radiat. Meas. 45 (10), 1305–1308. http://dx.doi.org/10.1016/j.radmeas.2010.06.043.

Hayes, S., Gamage, K., 2013. Scintillator based coded-aperture imaging for neutron detection. In: 3rd International Conference on Advancements in Nuclear Instrumentation Measurement Methods and their Applications (ANIMMA), pp. 1–6. http://dx.doi.org/10.1109/ANIMMA.2013.6727996.

Hirota, M., Takada, C., Takasaki, K., Momose, T., Kurihara, O., Saze, T., Ito, S., Nishizawa, K., 2011. Feasibility of in vivo measurement of ^{239}Pu distribution in lungs using an imaging plate. Appl. Radiat. isotopes 69 (5), 808–813. http://dx.doi.org/10.1016/j.apradiso.2011.01.018.

Hong, J., Vadawale, S.V., Zhang, M., Bellm, E.C., Yousef, A., Noss, J., Grindlay, J.E., Narita, T., 2004. Laboratory coded aperture imaging experiments: radial hole coded masks and depth-sensitive CZT detectors. In: Proceedings SPIE, Hard X-Ray and Gamma-Ray Detector Physics VI 5540, pp. 1–10. http://dx.doi.org/10.1117/12.559650.

Hughes, K.A., Mottershead, G., Thornley, D.J., Comrie, A.P., Group, O., 2004. Use of gamma-ray imaging instrumentation in support of TRU waste characterization challenges. In: Waste Management Conference, Tucson, AZ, pp. 1–9.

Inradoptics, Stilbene Single Crystals, Data sheet. URL http://inradoptics.com/products/scintillation-crystals/stilbene-single-crystals.

International Organization for Standardization, August 2001. Reference Neutron Radiations — Part 1: Characteristics and Methods of Production, Standard, BS ISO 8529-1:2001. British Standards Institution, London, UK.

Islamian, J., Azazrm, A., Mahmoudian, B., Gharapapagh, E., 2015. Advances in pinhole and multi-pinhole collimators for single photon emission computed tomography imaging. World J. Nucl. Med. 14 (1), 3–9. http://dx.doi.org/10.4103/1450-1147.150505.

Ivanov, O., Sudarkin, A., Stepanov, V., Urutskoev, L., 1999. Portable x-ray and gamma-ray imager with coded mask: performance characteristics and methods of image reconstruction. Nucl. Instrum. Methods Phys. Res. Sect. A Accel. Spectrom. Detect. Assoc. Equip. 422 (1–3), 729–734. http://dx.doi.org/10.1016/S0168-9002(98)01026-2.

Jahoda, K., Markwardt, C.B., Radeva, Y., Rots, A.H., Stark, M.J., Swank, J.H., Strohmayer, T.E., Zhang, W., 2006. Calibration of the rossi x-ray timing explorer proportional counter array. Astrophys. J. Suppl. Ser. 163, 401–423. http://dx.doi.org/10.1086/500659.

Joyce, M.J., Aspinall, M.D., Cave, F.D., Lavietes, A., 2014. A 16-channel real-time digital processor for pulse-shape discrimination in multiplicity assay. IEEE Trans. Nucl. Sci. 61 (4), 2222–2227. http://dx.doi.org/10.1109/TNS.2014.2322574.

Knoll, G.F., 2010. Radiation Detection and Measurement, fourth ed. John Wiley & Sons, Hoboken.

Kouzes, R.T., Ely, J.H., Erikson, L.E., Kernan, W.J., Lintereur, A.T., Siciliano, E.R., Stephens, D.L., Stromswold, D.C., Van Ginhoven, R.M., Woodring, M.L., 2010. Neutron detection alternatives to ^{3}He for national security applications. Nucl. Instrum. Methods Phys. Res. Sect. A Accel. Spectrom. Detect. Assoc. Equip. 623 (3), 1035–1045. http://dx.doi.org/10.1016/j.nima.2010.08.021.

Lilley, J., 2001. Nuclear Physics: Principles and Applications, Manchester Physics Series. J. Wiley.

Liu, G., Joyce, M.J., Ma, X., Aspinall, M.D., 2010. A digital method for the discrimination of neutrons and γ-rays with organic scintillation detectors using frequency gradient analysis. IEEE Trans. Nucl. Sci. 57 (3), 1682–1691. http://dx.doi.org/10.1109/TNS.2010.2044246.

MacWilliams, F.J., Sloane, N.J.A., 1976. Pseudo-random sequences and arrays. Proc. IEEE 64 (12), 1715–1729. http://dx.doi.org/10.1109/PROC.1976.10411.

Marleau, P., Brennan, J., Krenz, K., Mascarenhas, N., Mrowka, S., 2007. Advances in imaging fission neutrons with a neutron scatter camera. In: Nuclear Science Symposium Conference Record, 2007. NSS '07, vol. 1. IEEE, pp. 170–172. http://dx.doi.org/10.1109/NSSMIC.2007.4436310.

Marleau, P., Brennan, J., Brubaker, E., Hilton, N., Steele, J., 2009. Active coded aperture neutron imaging. In: 2009 IEEE Nuclear Science Symposium Conference Record (NSS/MIC), pp. 1974–1977. http://dx.doi.org/10.1109/NSSMIC.2009.5402146.

Marleau, P., Brennan, J., Brubaker, E., Steele, J., 2010. Results from the coded aperture neutron imaging system. In: Nuclear Science Symposium Conference Record (NSS/MIC), 2010 IEEE, pp. 1640–1646. http://dx.doi.org/10.1109/NSSMIC.2010.5874054.

Mascarenhas, N., Brennan, J., Krenz, K., Lund, J., Marleau, P., Rasmussen, J., Ryan, J., Macri, J., 2006. Development of a neutron scatter camera for fission neutrons. In: 2006 IEEE Nuclear Science Symposium Conference Record 2(2), pp. 185–188. http://dx.doi.org/10.1109/NSSMIC.2006.356135.

Masumoto, K., Toyoda, A., Eda, K., Ishihara, T., 2002. Measurement of the spatial distribution of neutrons in an accelerator room by the combination of activation detectors and an imaging plate. Radiat. Saf. Manag. 1 (1), 12–16.

Mortimer, R., Anger, H., Tobias, C., U. A. E. Commission, 1954. The Gamma-ray Pinhole Camera with Image Amplifier. U.S. Atomic Energy Commission. UCRL, University of California Radiation Laboratory.

Nakamura, T., Schooneveld, E., Rhodes, N., Katagiri, M., Sakasai, K., Soyama, K., 2009. Evaluation of the performance of a fibre-coded neutron detector with a ZnS^{10}/B_2O_3 ceramic scintillator. Nucl. Instrum. Methods Phys. Res. Sect. A Accel. Spectrom. Detect. Assoc. Equip. 600 (1), 164–166. http://dx.doi.org/10.1016/j.nima.2008.11.117.

Ott, R.J., MacDonald, J., Wells, K., Ott, R.J., 2000. The performance of a ccd digital autoradiography imaging system. Phys. Med. Biol. 45 (7), 2011. http://dx.doi.org/10.1088/0031-9155/45/7/322.

Peerani, P., Tomanin, A., Pozzi, S., Dolan, J., Miller, E., Flaska, M., Battaglieri, M., De Vita, R., Ficini, L., Ottonello, G., Ricco, G., Dermody, G., Giles, C., 2012. Testing on novel neutron detectors as alternative to ^{3}He for security applications. Nucl. Instrum. Methods Phys. Res. Sect. A Accel. Spectrom. Detect. Assoc. Equip. 696, 110–120. http://dx.doi.org/10.1016/j.nima.2012.07.025.

Pelowitz, D.B., April 2011. MCNPX User's Manual - Version 2.7.0.

Poularikas, A., 2006. Signals and Systems Primer with MATLAB, Electrical Engineering & Applied Signal Processing Series. Taylor & Francis.

Rees, L.B., Czirr, J.B., 2012. Optimizing moderation of He-3 neutron detectors for shielded fission sources. Nucl. Instrum. Methods Phys. Res. Sect. A Accel. Spectrom. Detect. Assoc. Equip. 691, 72–80. http://dx.doi.org/10.1016/j.nima.2012.07.004.

Santo, J.T., Maul, M., Lucero, Y., Clapham, M., Battle, B., Sluszka, D., Carberry, B., 2006. Application of Remote Gamma Imaging Surveys at the Turkey Point PWR Reactor Facility.

Schuster, P., Brubaker, E., 2015. Investigating the Anisotropic Scintillation Response in Anthracene through Neutron, Gamma-ray, and Muon Measurements, pp. 1–11. http://arxiv.org/abs/1511.00081.

Soppera, M.B.N., Dupont, E., 2012. Book of Neutron Comparison of Evaluated and Experimental Data, No. June. Nuclear Energy Agency. http://www.oecd-nea.org/janis/book/book-neutron.pdf.

Sudarkin, A.N., Ivanov, O.P., Stepanov, V.E., Volkovich, A.G., Turin, A.S., Danilovich, A.S., Rybakov, D.D., Urutskoev, L.I., 1996. High-energy radiation visualizer (HERV): a new system for imaging in x-ray and gamma-ray emission regions. IEEE Trans. Nucl. Sci. 43 (4), 2427–2433. http://dx.doi.org/10.1109/23.531792.

Sudarkin, A., Ivanov, O., Stepanov, V., Urutskoev, L., 1998. Portable gamma-ray imager and its application for the inspection of the near-reactor premises contaminated by radioactive substances. Nucl. Instrum. Methods Phys. Res. Sect. A Accel. Spectrom. Detect. Assoc. Equip. 414 (2–3), 418–426. http://dx.doi.org/10.1016/S0168-9002(98)00305-2.

Sun, S., Zhang, Z., Shuai, L., Li, D., Wang, Y., Liu, Y., Huang, X., Tang, H., Li, T., Chai, P., Jiang, X., Ma, B., Zhu, M., Wang, X., Zhang, Y., Zhou, W., Zeng, F., Guo, J., Sun, L., Yang, M., Zhang, Y., Wei, C., Ma, C., Wei, L., 2015. Development of a panorama coded-aperture gamma camera for radiation detection. Radiat. Meas. 77 (0), 34–40. http://dx.doi.org/10.1016/j.radmeas.2015.04.014.

Tous, J., Blazek, J., Zemlicka, J., Jakubek, J., 2011. Evaluation of a YAG: Ce scintillation crystal based CCD X-ray imaging detector with the Medipix2 detector. J. Instrum. 6 (11) http://dx.doi.org/10.1088/1748-0221/6/11/C11011. C11011–C11011.

Tremsin, A.S., Hussey, D.S., Downing, R.G., Feller, W.B., Mildner, D.F.R., Jacobson, D.L., Arif, M., Siegmund, O.H.W., 2005. Neutron collimation with microchannel plates: calibration of existing technology and near future possibilities. IEEE Trans. Nucl. Sci. 54 (2), 1–5. http://dx.doi.org/10.1109/NSSMIC.2005.1596220.

Tumerl, T., Neilll, T.J.O., Hurley, K., Ogelman, H., Paulos, R.J., Puettefl, R.C., Qpniss, I., Hamilton, W.J., Proctor, R., 1997. All-sky x-ray & gamma-ray astronomy monitor (AXGAM). IEEE Trans. Nucl. Sci. 44 (3), 572–576. http://dx.doi.org/10.1109/23.603713.

Vadawale, S.V., Hong, J., Grindlay, J.E., Skinner, G., 2005. Monte-Carlo simulations of the expected imaging performance of EXIST high-energy telescope. In: Proceedings SPIE, Optics for EUV, X-Ray, and Gamma-Ray Astronomy II, vol. 5900, pp. 590014–590112. http://dx.doi.org/10.1117/12.617671.

Vanier, P.E., 2004. Improvements in coded aperture thermal neutron imaging. In: Proceedings SPIE, Penetrating Radiation Systems and Applications V 5199, pp. 124–131. http://dx.doi.org/10.1117/12.509864.

Woodring, M., Beddingfield, D., Souza, D., Entine, G., Squillante, M., Christian, J., Kogan, A., 2003. Advanced multi-dimensional imaging of gamma-ray radiation. Nucl. Instrum. Methods Phys. Res. Sect. A Accel. Spectrom. Detect. Assoc. Equip. 505 (1–2), 415–419. http://dx.doi.org/10.1016/S0168-9002(03)01111-2.

Woolf, R.S., Phlips, B.F., Hutcheson, A.L., Mitchell, L.J., Wulf, E.A., 2012. An active interrogation detection system (ACTINIDES) based on a dual fast neutron/gamma-ray coded aperture imager. In: 2012 IEEE Conference on Technologies for Homeland Security (HST), pp. 30–35. http://dx.doi.org/10.1109/THS.2012.6459822.

Woolf, R.S., Phlips, B.F., Hutcheson, A.L., Wulf, E.A., 2015. Fast-neutron, coded-aperture imager. Nucl. Instrum. Methods Phys. Res. Sect. A Accel. Spectrom. Detect. Assoc. Equip. 784, 398–404. http://dx.doi.org/10.1016/j.nima.2015.01.084. http://linkinghub.elsevier.com/retrieve/pii/S0168900215001242.

Wu, Y., Song, J., Zheng, H., Sun, G., Hao, L., Long, P., Hu, L., 2015. CAD-based Monte Carlo program for integrated simulation of nuclear system SuperMC. Ann. Nucl. Energy 82, 161–168. http://dx.doi.org/10.1016/j.anucene.2014.08.058.

Yong-Hao, C., Xi-Meng, C., Xiao-Dong, Z., Jia-Rong, L., Li, A., Jian-Xiong, S., Pu, Z., Xin-Hua, W., Chuan-Xin, Z., Tie, H., Jian, Y., 2014. Study of n-γ discrimination in low energy range (above 40 keVee) by charge comparison method with a BC501A liquid scintillation detector. Chin. Phys. C 38 (3), 036001. http://stacks.iop.org/1674-1137/38/i=3/a=036001.

Zaitseva, N., Rupert, B.L., Paweczak, I., Glenn, A., Martinez, H.P., Carman, L., Faust, M., Cherepy, N., Payne, S., 2012. Plastic scintillators with efficient neutron/gamma pulse shape discrimination. Nucl. Instrum. Methods Phys. Res. Sect. A Accel. Spectrom. Detect. Assoc. Equip. 668, 88–93. http://dx.doi.org/10.1016/j.nima.2011.11.071.

Zaitseva, N., Glenn, A., Carman, L., Martinez, H.P., Hatarik, R., Klapper, H., Payne, S., 2015. Scintillation properties of solution-grown trans-stilbene single crystals. Nucl. Instrum. Methods Phys. Res. Sect. A Accel. Spectrom. Detect. Assoc. Equip. 789, 8–15. http://dx.doi.org/10.1016/j.nima.2015.03.090.